INFLUENCE OF BACKUP BEARINGS AND SUPPORT STRUCTURE DYNAMICS ON THE BEHAVIOR OF ROTORS WITH ACTIVE SUPPORTS

p. 25

Annual Status Report for Research Grant Number NAG3-1507

submitted to:

National Aeronautics and Space Administration
Lewis Research Center
Cleveland, Ohio 44135

by

George T. Flowers, Ph.D
Assistant Professor

Department of Mechanical Engineering
Auburn University
Auburn University, AL 36849-5341
Phone: (205) 844-3330

June, 1994

INFLUENCE OF BACKUP BEARINGS AND SUPPORT STRUCTURE DYNAMICS ON THE BEHAVIOR OF ROTORS WITH ACTIVE SUPPORTS

Annual Status Report for Research Grant Number NAG3-1507

submitted to:

National Aeronautics and Space Administration
Lewis Research Center
Cleveland, Ohio 44135

by

George T. Flowers, Ph.D
Assistant Professor

Department of Mechanical Engineering
Auburn University
Auburn University, AL 36849-5341
Phone: (205) 844-3330

June, 1994

Progress to Date

This report documents the progress that has been made in the proposed research work over the past year. The goals for year one have been completed. In addition, substantial progress has been made toward fulfilling the goals of year two. Work has also begun on additional areas that have been identified.

The work that has been completed to date is:

Completed before semi-annual report

1. A simplified rotor model with a flexible shaft and backup bearings has been developed. The model is based upon the work of Ishii and Kirk. Parameter studies of the behavior of this model are currently being conducted.

2. A simple rotor model which includes a flexible disk and bearings with clearance has been developed and the dynamics of the model investigated. The study consists of simulation work coupled with experimental verification. The work is documented in the attached paper. A copy of the paper is included in the Appendix.

3. A rotor model based upon the T-501 engine has been developed which includes backup bearing effects. The dynamics of this model are currently being studied with the objective of verifying the conclusions obtained from the simpler models.

4. Parallel simulation runs are being conducted using an ANSYS based finite element model of the T-501 developed by Dr. Charles Lawrence.

Progress since semi-annual report

1. The magnetic bearing test rig is currently floating and dynamics/control tests are currently being conducted. Photographs of the various test rigs that have been assembled for experimental testing for this project are shown in Figures 1 - 3.

2. A paper has been written that documents the work using the T-501 engine model. The paper has been accepted for presentation at the **Symposium on Nonlinear and Stochastic Dynamics**, to be held at the 1994 ASME Winter Annual Meeting, November 13-18, 1994, Chicago, Illinois. A copy of the paper is included in the Appendix.

3. Work has continued with the simplified model. A paper that fully documents this work is currently being written and will be submitted to the **ASME Turbo Expo**, June 5-8, 1995, Houston, Texas.

4. The finite element model is currently being modified to include the effects of foundation dynamics.

5. A literature search for material on foil bearings has been conducted.

6. A finite element model is being developed for a magnetic bearing in series with a foil backup bearing.

Bibliography

1. Flowers, G.T., and Wu, Fangsheng, ''Disk/Shaft Vibration Induced by Bearing Clearance Effects: Analysis and Experiment,'' to be presented at the **Second Biennial European Joint Conference on Engineering Systems, Design, and Analysis (ESDA)**, July 4-7, London, England; submitted to *ASME Journal of Vibration and Acoustics*, February, 1994.

2. Flowers, G.T., Xie, Huajun, and Lawrence, C. ''Steady-State Dynamic Behavior of an Auxiliary Bearing Supported Rotor System,'' accepted for presentation at the **Symposium on Nonlinear and Stochastic Dynamics**, to be held at the 1994 ASME Winter Annual Meeting, November 13-18, 1994, Chicago, Illinois.

3. Flowers, G.T., Xie, Huajun, and Lawrence, C., ''Dynamics of a Rotor Supported by a Bearing With Clearance,'' abstract submitted to the **ASME Turbo Expo**, June 5-8, 1995, Houston, Texas.

4. Flowers, G.T., and Lawen, J., ''Influence of Rubbing on a Magnetic Bearing Supported Rotor System,'' abstract submitted to the **ASME Turbo Expo**, June 5-8, 1995, Houston, Texas.

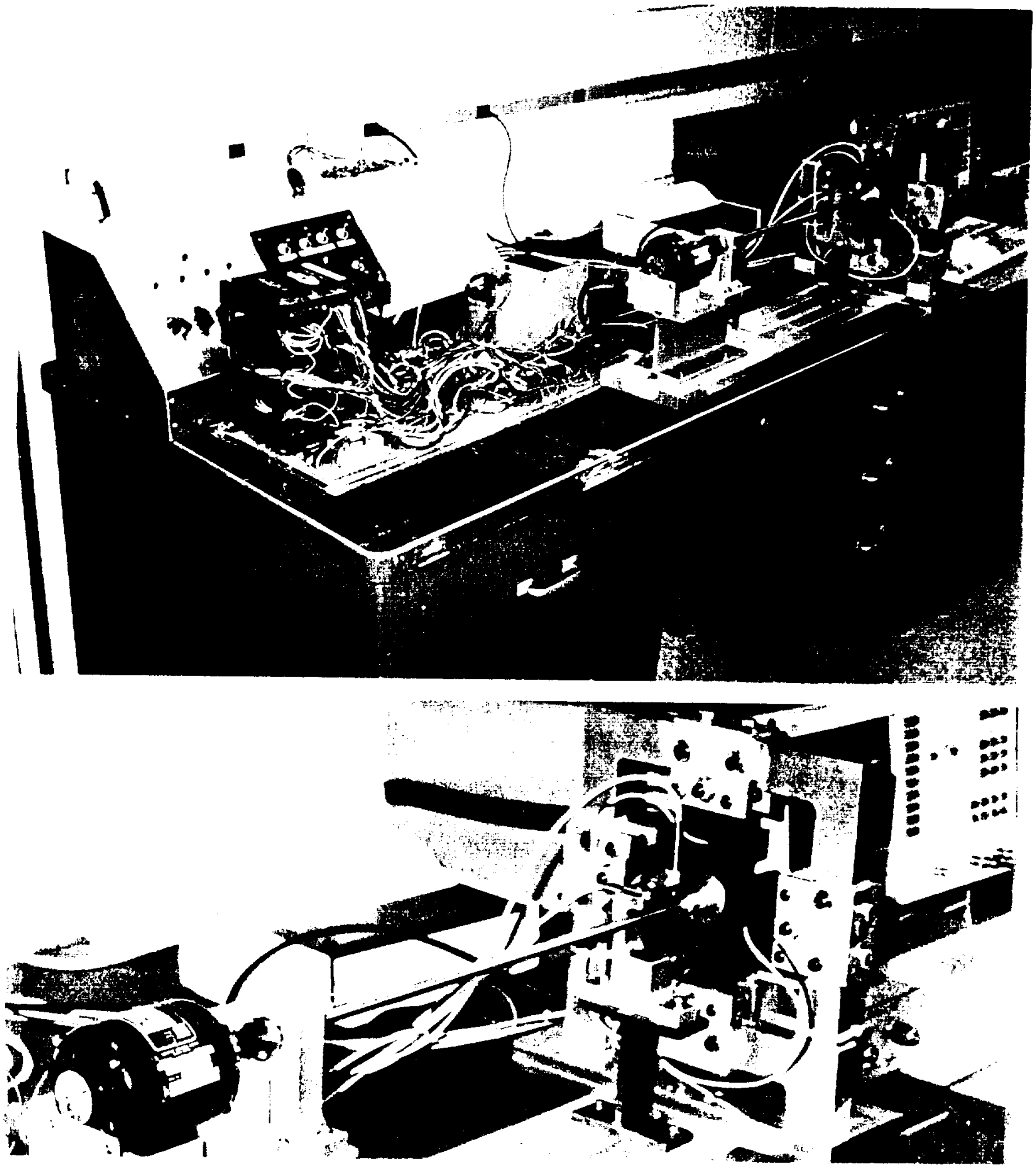

Figure 1: Magnetic Bearing Test Rig

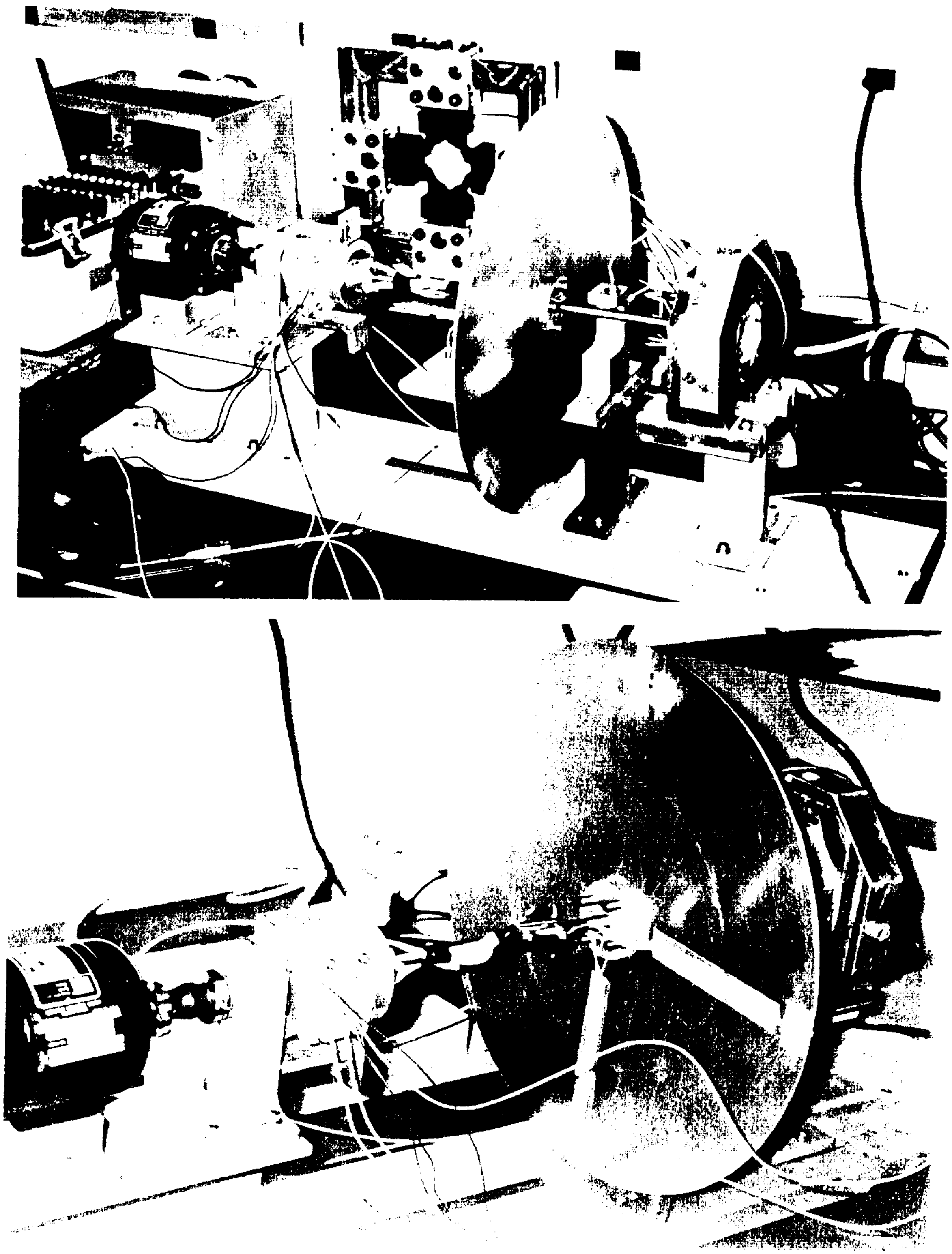

Figure 2: Flexible Disk Test Rig

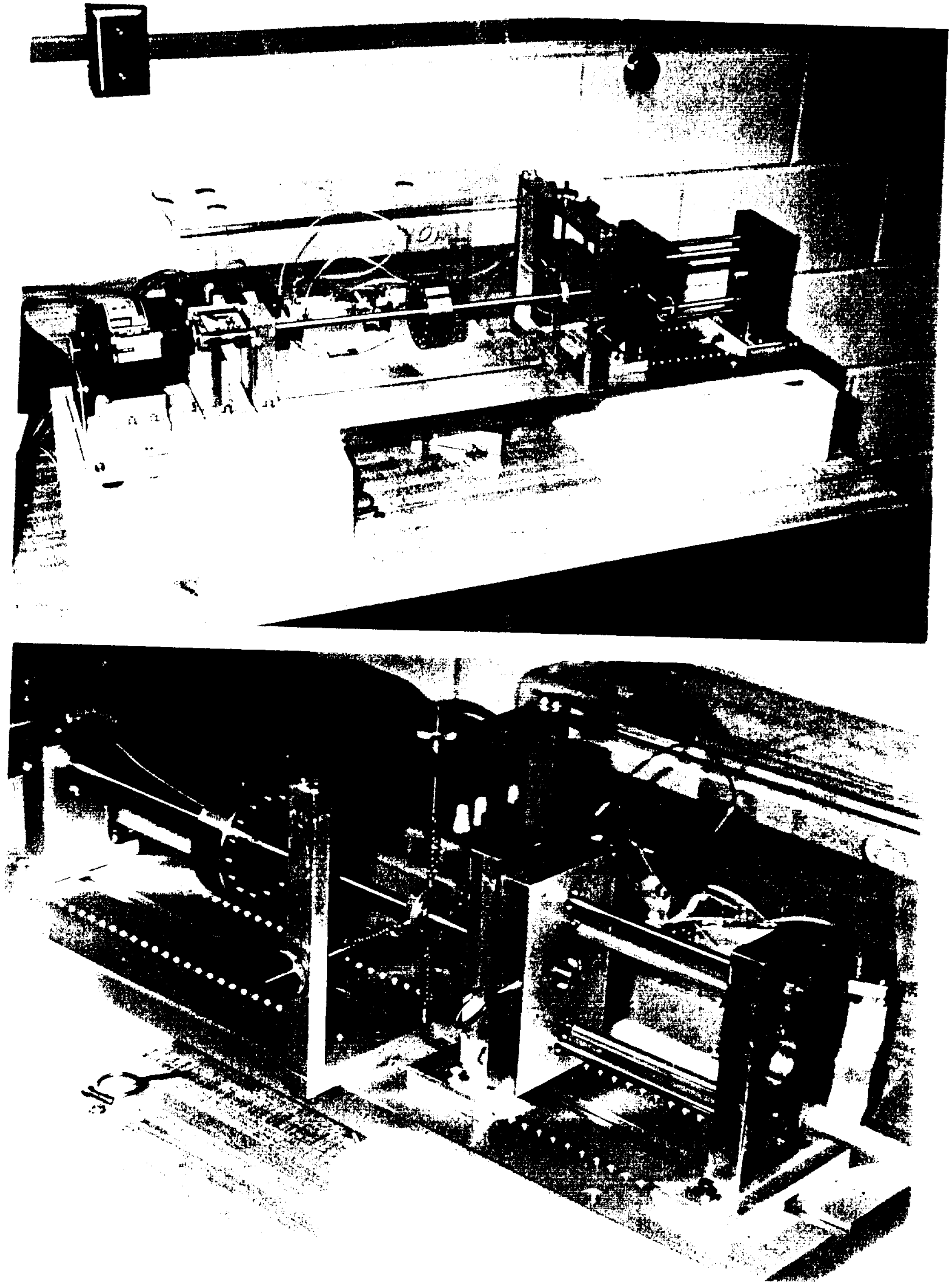

Figure 3: Transient Drop Rotordynamics Test Rig

Appendix

To be presented at

Second Biennial European Joint Conference on Engineering Systems, Design & Analysis
July 4-7, 1994
London, England

DISK/SHAFT VIBRATION INDUCED BY BEARING CLEARANCE EFFECTS: ANALYSIS AND EXPERIMENT

George T. Flowers
Fangsheng Wu

Department of Mechanical Engineering
Auburn University
Auburn, AL

Abstract

This study presents an investigation of the dynamics of a rotor system with bearing clearance. Of particular interest is the influence of such effects on coupled shaft/disk vibration. Experimental results for a rotor system with a flexible disk are presented and compared to predictions from a simulation model. Some insights and conclusions are obtained with regard to the conditions under which such vibration may be significant.

Nomenclature

e = imbalance eccentricity
f_{n1}, f_{n2} = nonlinear bearing forces
r_1 = gyroscopic mass influence ratio
r_2 = disk mass influence ratio
x_1, x_2 = shaft degrees of freedom
x_3, x_4 = disk degrees of freedom
Δ = bearing clearance
Ω = rotor speed
ω_1 = natural frequency of rotor support in x_1 direction
ω_2 = natural frequency of rotor support in x_2 direction
ω_3 = natural frequency of rotor disk
τ = Ωt
ξ_1 = damping ratio of rotor support in x_1 direction
ξ_2 = damping ratio of rotor support in x_2 direction
ξ_3 = damping ratio of rotor disk
$(\dot{\ }) = \frac{d}{d\tau}$

Background and Motivation

Rotor systems typically consist of a shaft with one or more bladed disks attached. Disk and blade vibration are issues of important concern for stress analysts. Complex finite element models are developed to assess the dynamic stresses in such components and insure the integrity of the design. However, models for rotordynamical analyses are typically developed assuming that disk flexibility effects are negligible. It is generally presumed that the disk is sufficiently rigid so as to not significantly impact rotor vibration over the operating region.

There is a fairly large body of work documented in the literature concerning studies of disk flexibility on rotors and turbomachinery. A discussion of this previous work with regard to linear rotor systems is presented in Flowers and Ryan (1991). An excellent source for a comprehensive review of work in this area is presented by Davis (1989).

Previous investigators into the area of coupled rotor/disk vibration have noted that disk flexibility has little effect on critical speeds but that it may significantly influence higher natural frequencies of the rotor system [Chivens and Nelson (1975)]. One can draw the conclusion from these results that synchronous vibration due to imbalance will be little affected by disk flexibility. However, there are sources of higher frequency excitation that could serve to excite these natural frequencies. Perhaps the most obvious are multi-synchronous effects corresponding to the blade pass frequency (from fluid forces impinging on the rotor blades). Another potential source is from nonlinearities that may be present in the system. For example, nonlinear bearing forces due to clearance effects may result in supersynchronous rotor vibration. There are quite a number of studies in the literature concerning the effects of bearing clearance (and the related phenomena of rubbing) on rotordynamical behavior. Some of the works that have most influenced the current study were conducted by Johnson (1962), Black (1968), Ehrich (1966), and Childs (1978), and Muszynska (1984).

Advanced designs for many types of high speed rotating machinery that use magnetic bearings for support have been proposed and are in the development and construction stages. There are a number of such systems already in commercial use. Rotor systems supported by magnetic bearings must have backup bearings to provide support under overload conditions or if the magnetic bearing fails. Backup bearings are characterized by a clearance between the rotor and the bearing such that contact does not occur under normal operating conditions. As a result, issues related to the effects of bearing clearance on rotordynamical behavior are of current concern. The objective of the present work is to develop an understanding of possible coupling between the dynamics of disk and shaft that may be induced by bearing clearance effects and to provide guidance to designers concerned with such systems.

Experimental Model

In order to investigate whether bearing clearance can lead to significant coupling between rotor and disk vibration, experimental tests were performed with a rotor test rig. A drawing of the test rig is shown in Figure 1.

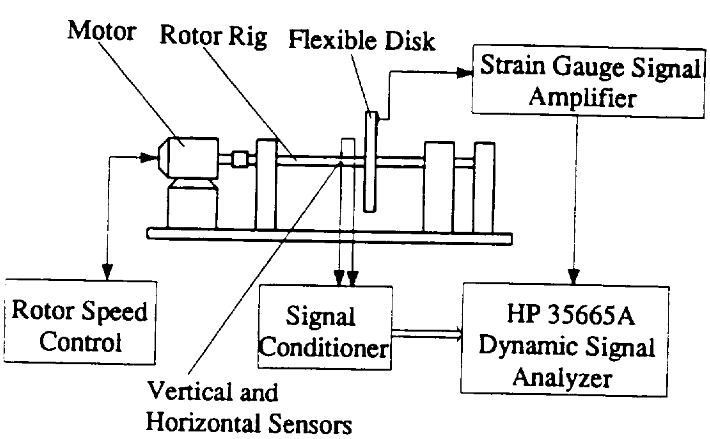

Figure 1 Experimental Test Apparatus

The rotor used in this study has two basic components: a flexible disk and a shaft. The steel shaft is 0.375 in. diameter and 18 inches long. The flexible disk is a circular aluminum plate 0.0125 inches thick and 14.0 inches in diameter. The natural frequency of its lowest one nodal diameter bending mode is about 40 Hz. It is attached with bolts to a 2.0 inch diameter hub that is fixed on at

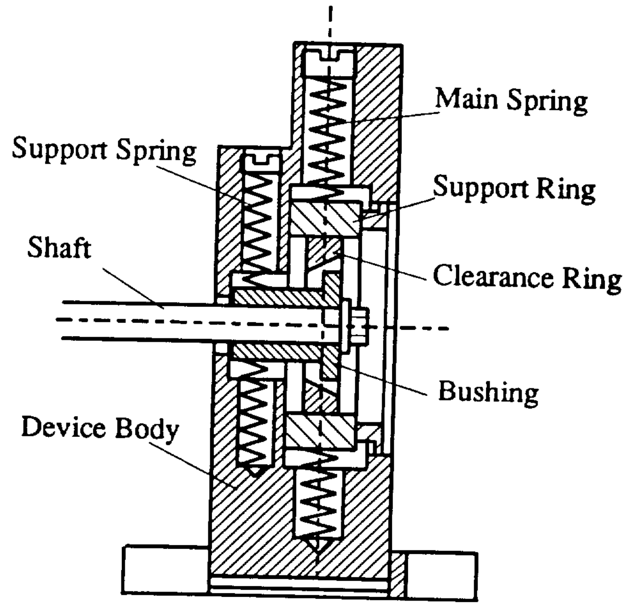

Figure 2 Shaft Right End Support Device

the center of a 0.375 inch diameter steel shaft 16.0 inches in length.

The rotor shaft is supported by bushings at two ends. The left end of the shaft is placed directly in the bushing base. This support provides a force but only a minimal couple so that the shaft is effectively free to pivot about this point. The right bearing is supported by a special device, which is designed to provide stiffness and to simulate bearing clearance. A diagram for this device is shown in figure 2. It has two sets of springs. The softer springs are to support the weight of the rotor, and the harder springs act as the main stiffness for the system. The stiffness in the x and y directions of each spring set may be different. The clearance is adjustable by turning the inner tapered ring in or out. In this experiment, the spring constant of the soft spring is 1.9 lb/in. The spring constant of the hard spring is 8.1 lb/in. in the x_1 (horizontal) direction and 19.7 lb/in. in the x_2 (vertical) direction.

The rotor is driven by a speed adjustable motor. The speed of the rotor can be controlled by turning the speed control knob on the front panel of the control box. The measurement and analysis system comprises proximity displacement sensors, sensor conditioners and a signal analyzer. A vertical and a horizontal displacement sensor were mounted to pick up the displacement signals to form orbit plots. A third transducer was used to sense the disk vibration. During the test, displacement signals of the shaft were sent to the signal analyzer, where the orbit trajectories were recorded and the frequency components of the vibration were analyzed.

Simulation Model

The simulation model is similar to that developed in an earlier study [Flowers and Wu (1993)]. The primary differences are that rotational stiffening of the disk have been taken into account and that damping is included in the bearing support forces. A schematic diagram of the model is shown in figure 3. It consists of a rigid shaft, a rigid hub, a flexible disk and a support with a symmetric clearance. The equation development is based on the following considerations:

(1) The disk is assumed to flex only in the lateral direction.
(2) Only rotational vibration is considered. This is because only the rotational motion is coupled with the lateral disk vibration. One nodal diameter disk vibration is assumed.
(3) The rotor speed is constant.

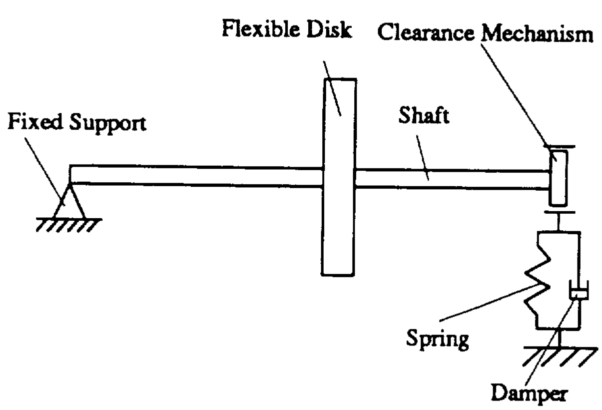

Figure 3 Simulation Model

After some mathematical manipulations, the dimensionless equations of motion for the whole system can be obtained as

$$\ddot{x}_1 + r_1\ddot{x}_2 + r_2\ddot{x}_3 + 2\dot{x}_4 + f_{n1} = \cos\tau \qquad (1)$$

$$\ddot{x}_2 - r_1\ddot{x}_1 + r_2\ddot{x}_4 - 2\dot{x}_3 + f_{n2} = \sin\tau \qquad (2)$$

$$\ddot{x}_3 + 2\dot{x}_4 + 2\xi_3\omega_3\dot{x}_3 + (\omega_3^2 - 1)x_3 = -(\ddot{x}_1 + 2\dot{x}_2) \qquad (3)$$

$$\ddot{x}_4 - 2\dot{x}_3 + 2\xi_3\omega_3\dot{x}_4 + (\omega_3^2 - 1)x_4 = -(\ddot{x}_2 - 2\dot{x}_1) \qquad (4)$$

$$f_{n1} = -\phi\left[(1 - \frac{\delta}{\sqrt{x_1^2 + x_2^2}})(\omega_1^2 x_1) + 2\xi_1\omega_1\dot{x}_1\right]$$

$$f_{n2} = -\phi\left[(1 - \frac{\delta}{\sqrt{x_1^2 + x_2^2}})(\omega_2^2 x_2) + 2\xi_2\omega_2\dot{x}_2\right]$$

$$\delta = \frac{\Delta}{e}$$

$$\phi = \begin{cases} 1 & \text{if} \sqrt{x_1^2 + x_2^2} > \delta \\ 0 & \text{otherwise} \end{cases}$$

In the above equations, x_1, x_2, x_3 and x_4 are scaled by e, the imbalance eccentricity. Time is scaled by the rotor speed, Ω. f_{n1} and f_{n2} are the nonlinear moments due to contacting between the rotor and the bearings.

The effective stiffness of a spinning disk can be strongly influenced by the spin speed. Based upon earlier work [Wu and Flowers (1992)], the lowest natural frequency of such a disk can be written as

$$\omega_3^2 = \frac{19 + \nu}{16} + \frac{\omega_{30}^2}{\Omega^2}$$

where ω_{30} is the natural frequency of the nonspinning disk. This expression is used in equations 3 and 4 to account for spin stiffening effects.

Comparison of Experiment and Simulation

A number of tests were conducted using the experimental setup described in the previous section. In addition, studies for differing parametric configurations have been conducted using the simulation model described above. The basic results are very similar to those obtained by Flowers and Wu (1993). The results presented here are typical. The following discussion is directed at comparing the predictions of the simulation model with experimentally observed responses, with the objective of obtaining insight into the behavior of flexible disk rotor systems with bearing clearance effects.

First, the linear characteristics of the system were examined. Figure 4 shows experimentally obtained data of the natural frequencies for the coupled disk/shaft vibration mode as a function of rotor speed. Using the data from such tests and additional measurements and calculations, the linear stiffness, damping, and mass characteristics of the experimental rotor system were identified. The numerical values are shown in Table 1.

Parameter	Value
r_1	0.5
r_2	0.1
ξ_1	0.06
ξ_2	0.06
ξ_3	0.01
ω_1	0.55
ω_2	0.85
ω_3	1.8
ν	0.3
δ	1.2

Table 1 Simulation Model Parameters

Figure 4 also shows the natural frequencies as a function of rotor speed obtained from the simulation model. These results agree relatively well with the experimentally obtained data and serve to validate the structural parameters selected for the simulation model. Ω, 3Ω, and 5Ω lines are also shown on the figure. The intersections of these lines with the natural frequency curve provides significant insight into the nonlinear behavior of the flexible disk rotor system, as is discussed below.

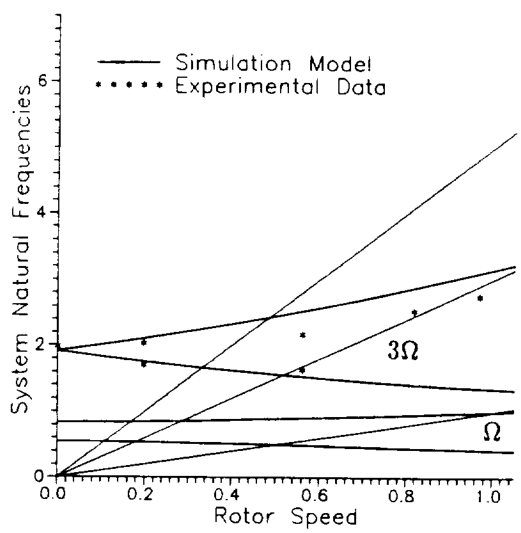

Figure 4 Rotor System Natural Frequencies

Next, the nonlinear behavior of the system was investigated. A clearance value was selected and the rotor speed was slowly increased over a range of rotor speeds, with the resulting response amplitudes and frequencies measured and recorded.

It is important to note that many vibration frequencies are possible. During the course of the study, 1Ω – $6\ \Omega$ frequency components were observed for certain parametric configurations. In addition, frequency components that are fractions of the rotor speed were observed for certain speed ranges and initial conditions. However, for a rotor with a symmetric clearance and minimal frictional effects, the odd integer multiples of the rotor speed appear to generally be the primary supersynchronous frequency components. The current discussion will concentrate on those frequencies. However, the basic conclusions should be directly applicable to other supersynchronous vibration frequencies as well.

Figure 5 shows the experimentally measured amplitudes of the Ω, 3Ω, and 5Ω components of the shaft response for various rotor speeds. Simulation results are also shown on figure 5. These results were obtained using the harmonic balance method and were verified at selected points through direct numerical integration of the equations of motion. There is relatively good agreement between the simulation results and the corresponding experimental data. Certainly the basic trends match quite well.

An important observation that can be made from examination of these figures is that the peaks of the respective components correspond to the the intersections of the Ω, 3Ω, and 5Ω lines with the natural frequency curves. It appears that the nonlinear effects are serving to excite the coupled modes of the rotor/disk system. This is true for both the forward and backward whirl modes of the rotor system.

The peaks occurring at a rotor speed of 0.51 correspond to the intersections of the 3Ω line with the natural frequency curve. They relate to a backward whirl mode. The peaks occurring at rotor speeds of 0.33 and 0.485 correspond to the intersections of the 5Ω line with the the natural frequency curve. Those occurring at 0.33 relate to a backward whirl mode and those occurring at 0.485 relate to a forward whirl mode. Note that the amplitudes of the supersynchronous components associated with the forward whirl mode of the disk/shaft vibration are much lower than those associated with the backward whirl mode. This result was observed for all the parametric configurations examined in the course of this study.

The Ω, 3Ω, and 5Ω components contribute (more or less significantly) to the overall response at the corresponding intersection point. However, it is important to note that the Ω component is increased rather dramatically at the intersection points as a result of the presence of disk flexibility. Apparently, the nonlinear coupling between the various frequency components serves to produce this effect.

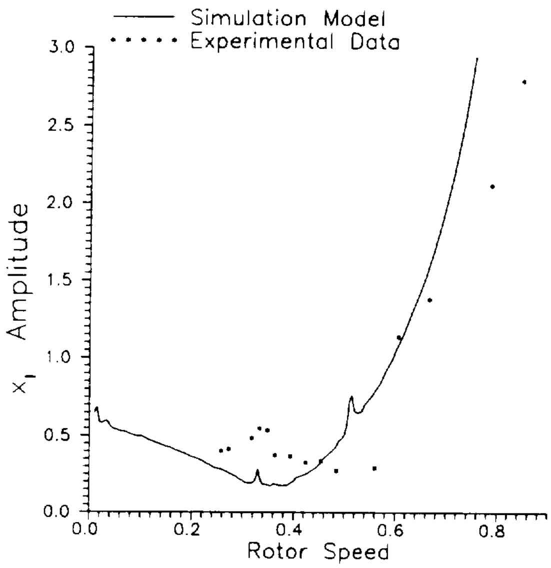

Figure 5.a Ω Component of Shaft Vibration Response

Conclusions

A study of disk/shaft vibration induced by bearing clearance effects has been presented. Both experimental tests and simulation results have been presented. The responses predicted by the simulation model and those observed experimentally agree quite well. The behavior of both the experimental test rig and the simulation model was quite sensitive to changes in parametric configuration. As a result it is quite difficult to predict exactly how a certain system is going to behave in the presence of a bearing clearance effect, i.e., whether or not coupled disk/shaft vibration will be significantly excited. However, a few general conclusions and guidelines can be drawn from this study.

1. An understanding of the mechanism for coupled disk/shaft vibration induced by clearance effects has been obtained. The nonlinear effects have served to produce superharmonics that excite coupled disk shaft modes. Conversely, the additional degree of freedom pro-

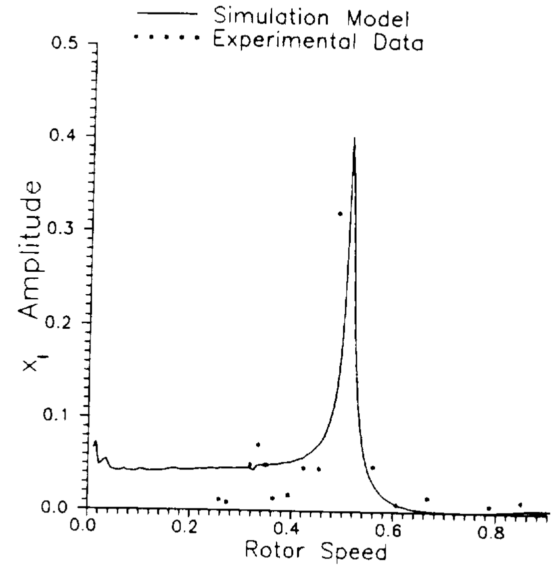

Figure 5.b 3Ω Component of Shaft Vibration Response

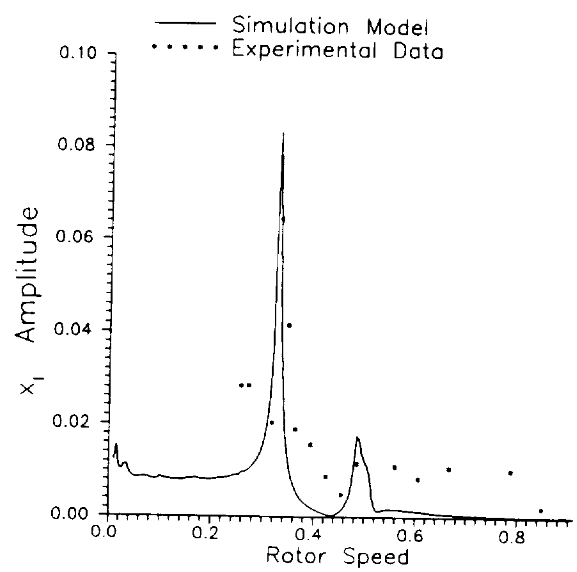

Figure 5.c 5Ω Component of Shaft Vibration Response

vided by the disk flexibility has served to exaggerate the frequency components of the response, resulting in higher amplitudes at the rotor speeds corresponding to the respective natural frequency/multi-synchronous line intersection points.

2. Bearing clearance effects primarily serve to excite backward whirl modes for coupled disk/shaft vibration. Forward whirl modes may be excited but the associated amplitudes appear to be much lower.

3. The bearing support stiffnesses used in this study were not symmetric. These nonsymmetries, together with the clearance, have served to produce the supersynchronous vibration that excites the coupled disk/shaft vibration modes.

4. It appears to be relatively difficult to excite coupled disk/shaft vibration with bearing clearance effects. The occurrence of such behavior was very sensitive to rotor speed, as judged by the relative difficulty encountered during the experimental work in obtaining the peak amplitude responses. This conclusion is verified by the simulation work that indicates that the behavior occurs only over a very limited ranges of rotor speed. The supersynchronous frequency must almost exactly coincide with a natural frequency in order to excite the behavior.

5. From a design perspective, the Campbell diagram is a useful tool to predict when such behavior may occur. The intersections of the corresponding supersynchronous line with the coupled disk/shaft vibration mode frequency curve will indicate at what rotor speeds peak responses for that frequency component are likely to occur. Whether or not such behavior will actually occur and the relative significance of such effects depends very strongly on the imbalance, clearance, damping, and stiffness values.

Acknowledgement

This work was partially supported by the National Science Foundation under Grant No. MSS-9110051 and partially by the National Aeronautics and Space Administration under Grant No. NAG3-1507. The Government has certain rights in this material. Special appreciation is expressed to Dr. Charles Lawrence of NASA/Lewis Research Center.

References

Black, H.F., "Forced Subrotative Speed Dynamic Action of Rotating Machines," *Journal of Mechanical Engineering Science*, Vol. 10, No. 4, pp. 1–12.

Chivens, D.R., and Nelson, H.D., "The Natural Frequencies and Critical Speed of a Rotating, Flexible Shaft–Disk System," *ASME Journal of Engineering for Industry*, Vol. 97, August, 1975, pp. 881–886.

Childs, D.W., "Rub–Induced Parametric Excitation in Rotors," ASME Paper No. 78–WA/DE–14, Presented at the 1978 ASME Winter Annual Meeting.

Davis, R.R., "Practical Nonlinear Simulation of Rotating Machinery Dynamics with Application to Turbine Blade Rubbing ," Ph.D. Dissertation, Department of Mechanical Engineering, University of California, Davis June 1989.

Ehrich, F.F., "Subharmonic Vibrations of Rotors in Bearing Clearance," ASME Paper 66-MD-1, Design Engineering Conference and Show, Chicago, Ill, May 9-12, 1966.

Flowers, G.T. and Ryan, S.G, "Development of a Set of Equations for Incorporating Disk Flexibility Effects in Rotordynamical Analyses ," *ASME Journal of Engineering for Gas Turbines and Power*, Vol. 115, No. 2, 1993, pp. 227–233.

Flowers, G.T. and Wu, F.S. "A Study of the Influence of Bearing Clearance on Lateral Coupled Shaft/Disk Rotordynamics," Rotordynamical Analyses ," *ASME Journal of Engineering for Gas Turbines and Power*, Vol. 115, No. 2, 1993, pp. 279–286.

Johnson, D.C., "Synchronous Whirl of a Vertical Shaft Having a Clearance in One Bearing," *Journal of Mechanical Engineering Science*, Vol. 4, No. 1, 1962, pp. 85–93.

Lamb, H., and Southwell R.V., " The Vibrations of a Spinning Disk," *Proceedings of the Royal Society of London*, Series A, Vol. 99, July, 1921, pp. 272–280.

Muszynska, A., "Synchronous and Self–Excited Vibrations Caused by Full Annular Rub," presented at *Eigth Machinery Dynamics Seminar*, Halifax, Nova Scotia, Canada, Oct. 1–2, 1984.

Wu, F.S., and Flowers, G.T., "A Transfer Matrix Technique for Evaluating the Natural Frequencies and Critical Speeds of a Rotor with Multiple Flexible Disks," *ASME Journal of Vibration and Acoustics*, Vol. 114, No. 2, 1992, pp. 242–248.

To be presented at

Symposium on Nonlinear and Stochastic Dynamics

to be held at the 1994 ASME Winter Annual Meeting
November 13-18, 1994
Chicago, Illinois

STEADY-STATE DYNAMIC BEHAVIOR OF AN AUXILIARY BEARING SUPPORTED ROTOR SYSTEM

Huajun Xie and George T. Flowers

Department of Mechanical Engineering
Auburn University
Auburn, Alabama

Charles Lawrence

NASA Lewis Research Center
Cleveland, Ohio

ABSTRACT

This paper investigates the steady-state responses of a rotor system supported by auxiliary bearings in which there is a clearance between the rotor and the inner race of the bearing. A simulation model based upon the rotor of a production jet engine is developed and its steady-state behavior is explored over a wide range of operating conditions for various parametric configurations. Specifically, the influence of rotor imbalance, support stiffness and damping is studied. It is found that imbalance may change the rotor responses dramatically in terms of frequency contents at certain operating speeds. Subharmonic responses of 2nd order through 10th order are all observed except the 9th order. Chaotic phenomenon is also observed. Jump phenomena (or double-valued responses) of both hard-spring type and soft-spring type are shown to occur at low operating speeds for systems with low auxiliary bearing damping or large clearance even with relatively small imbalance. The effect of friction between the shaft and the inner race of the bearing is also discussed.

NOMENCLATURE

C_B = auxiliary bearing support damping, lb.s^2/in.
$C_{B\psi}$ = auxiliary bearing torsional damping, lb.in.s
F_n = normal force, lb
F_t = friction force, lb
$\mathbf{F}_X$ = external force vector acting on the rotor in X direction
$\mathbf{F}_Y$ = external force vector acting on the rotor in Y direction
$\mathbf{I}_a$ = rotor inertia matrix
J_B = moment of inertia of auxiliary bearing, lb.in.s^2
K_B = auxiliary bearing support stiffness, lb/in.
K_C = contact stiffness, lb/in.
M_B = auxiliary bearing mass, lb.s^2/in.
M_k = mass of kth rotor element, lb.s^2/in.
N = total number of modes considered
$NB1$ = node number at auxiliary bearing #1
$NB2$ = node number at auxiliary bearing #2
$\mathbf{Q}_X$ = rotor modal coordinate vector in X direction
$\mathbf{Q}_Y$ = rotor modal coordinate vector in Y direction
R_B = radius of auxiliary bearing bore, in.
R_m = radius of auxiliary bearing pitch, in.
R_R = radius of rotor journal, in.
$\mathbf{X}_R$ = rotor physical coordinate vector in X direction
$\mathbf{Y}_R$ = rotor physical coordinate vector in Y direction
e = rotor imbalance eccentricity, in.
g = gravitational acceleration, in./s^2
t = time, s
Δ = deformation at the contact point, in.
$\mathbf{\Gamma} = \mathbf{\Psi}^T \mathbf{I}_a \mathbf{\Psi}$
$\mathbf{\Psi}$ = rotor free-free modal rotation matrix
Ω = rotor operating speed, rad/s
$\mathbf{\Phi}$ = rotor free-free modal displacement matrix
$\delta = R_B - R_R$, auxiliary bearing clearance, in.
μ = dynamic friction coefficient
μ_ψ = rolling friction coefficient
ψ_B = angular displacement of auxiliary bearing inner-race
ζ = modal damping coefficient

INTRODUCTION

One of the most innovative developments in the turbomachinery field involves the use of active magnetic bearings (AMB) for rotor support. This technology provides the potential for significant improvements in the dynamic behavior of rotor systems, allowing for loading, eccentricity, shaft position and vibration to be continuously monitored and controlled. In order to protect the soft iron cores of the magnetic bearings and to provide rotor support in the event of failure of the bearing or during an overload situation, backup (or auxiliary) bearings, with a clearance between the rotor and the inner race of the bearing, are usually included in the rotor design. This clearance introduces a nonlinear dynamical feature which may significantly impact the behavior of the rotor.

Magnetic bearing systems appear to provide particularly great promise for use in aerospace applications. There are active programs at many of the major jet engine manufacturers to develop engines supported by magnetic bearings. Safety is a major concerns in any aeronautical design. Toward this end, it is desirable to design the rotor system to take maximum advantage of the backup bearings and use them as true auxiliary bearings to provide support during critical situations in a safe and consistent manner. An important concern in this regard is the dynamic behavior of the rotor when it comes into contact with the auxiliary bearing. If safe and effective operation of the engine is to be ensured during these periods, it is essential that designers have a very good understanding of the steady-state dynamics of rotor systems with clearance effects.

There are a number of studies in the literature concerned with the dynamics of rotors with clearance effects. Yamamoto (1954) conducted a systematic study of rotor responses involving bearing clearance effects. Black (1968) studied the rotor/stator interaction with a clearance. He concluded that rotor/stator interactions may occur in a variety of forms and circumstances, including jump phenomena. Ehrich (1966) reported the first identification of a second order subharmonic vibration phenomenon in a rotor system associated with bearing clearance (1966). Bently (1974) published experimental observations of second and third order subharmonic vibration in a rotor system. Later, Muszynska (1984) cited the occurrence of second, third, and fourth order subharmonic responses in a rotor rubbing case and Ehrich (1988 and 1991) observed eighth and ninth order subharmonic vibration as well as chaotic vibration in a high speed turbomachine. Childs (1979 and 1982) published two papers to explain the mechanism for the second and third order subharmonic responses noted above. He stated, with great insight, that " motion due to nonsymmetric clearance effects is a fractional-frequency phenomenon."

While those studies have greatly enhanced the understanding of clearance effects on rotor dynamics, a more detailed understanding of the dynamical behavior of such systems is needed. The perspective of much of this earlier work is that the clearance exists as a result of manufacturing error or misfitting. That is, it is due to an abnormal situation. However, in a rotor system fitted with magnetic bearings and auxiliary bearings, the clearance becomes a design parameter rather than an irregularity. From this point of view, it is important to develop a detailed quantitative understanding of the dynamic responses that are to be expected. Such knowledge will provide guidelines for the selection of auxiliary bearing parameters.

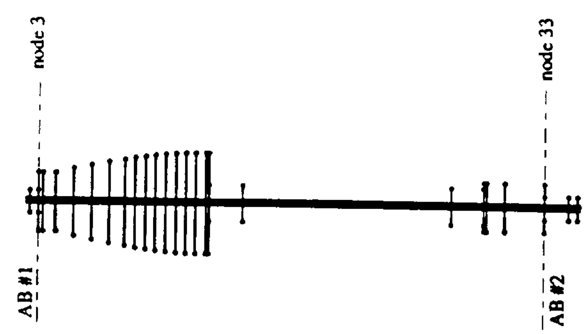

FIG. 1 DIAGRAM OF THE FEM ROTOR MODEL

It seems that there have been little work to date that is specifically concerned with auxiliary bearings in magnetic bearing supported rotor systems. Two papers that are directly related to research on auxiliary bearings were both focused on transient responses. Gelin et al. (1990) studied the transient dynamic behavior of rotors on auxiliary bearings during the coast down. Ishii and Kirk (1991) investigated the transient responses of a flexible rotor during the rotor drop after the magnetic bearings become inactive. In both papers, idealized rotor models are used and it is assumed that once the magnetic bearings fail, the torque is cut off and consequently the rotor speed approaches zero.

In this paper, simulation results are presented for a complex rotor system supported by auxiliary bearings with clearance at each end of the rotor. This work is specifically concerned with systems in which the clearances are quite small (on the order of a few mils), which is appropriate for jet engine applications in which the backup bearing is acting to provide rotor support on a consistent basis. The influence of rotor imbalance, support stiffness and support damping are investigated using direct numerical integration of the governing equations of motion and the harmonic balance method. Some insights are obtained with regard to the frequency and amplitude behavior of the steady-state vibration of such a system.

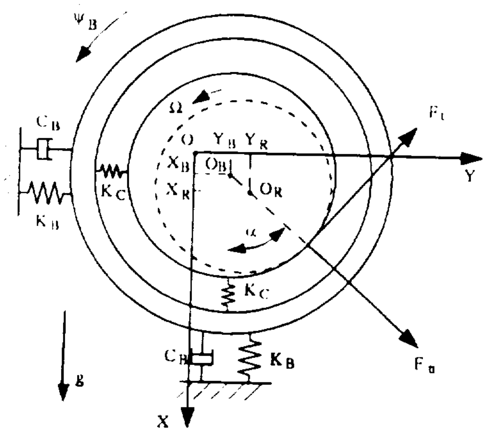

FIG. 2 AUXILIARY BEARING MODEL

SIMULATION MODEL

The rotor is modelled using free–free normal mode shapes and natural frequencies obtained through finite element analysis. The model data is representative for the rotor of a jet engine. Fig. 1 shows a schematic diagram of the FEM rotor model. Parametric information about the model is listed in Table 1. The torsional motion of the shaft is not considered in this paper. Using state space representation and modal coordinates, the equations of motion for the rotor are expressed as

$$\begin{aligned} \ddot{\mathbf{Q}}_X + 2\zeta\omega_n\dot{\mathbf{Q}}_X + \Omega\Gamma\dot{\mathbf{Q}}_Y + \omega_n^2\mathbf{Q}_X \\ + 2\Omega\zeta\omega_n\mathbf{Q}_Y = \mathbf{\Phi}^T\mathbf{F}_X, \end{aligned} \qquad (1.a)$$

$$\begin{aligned} \ddot{\mathbf{Q}}_Y + 2\zeta\omega_n\dot{\mathbf{Q}}_Y - \Omega\Gamma\dot{\mathbf{Q}}_X + \omega_n^2\mathbf{Q}_Y \\ - 2\Omega\zeta\omega_n\mathbf{Q}_X = \mathbf{\Phi}^T\mathbf{F}_Y, \end{aligned} \qquad (1.b)$$

where

$$\begin{aligned} \mathbf{F}_X &= \{F_{X1}, F_{X2}, \dots, F_{Xm}\}^{-1}, \\ \mathbf{F}_Y &= \{F_{Y1}, F_{Y2}, \dots, F_{Ym}\}^{-1}, \\ \mathbf{Q}_X &= \mathbf{\Phi}^{-1}\mathbf{X}_R, \\ \mathbf{Q}_Y &= \mathbf{\Phi}^{-1}\mathbf{Y}_R, \end{aligned}$$

with

$$\begin{aligned} \mathbf{X}_R &= \{X_{R1}, X_{R2}, \dots, X_{Rm}\}^{-1}, \\ \mathbf{Y}_R &= \{Y_{R1}, Y_{R2}, \dots, Y_{Rm}\}^{-1}. \end{aligned}$$

(m = total number of nodes)

The physical displacements of the rotor at the two auxiliary bearing locations can be obtained using the following coordinate transformation:

$$X_{Rk} = \sum_{i=1}^{N} \Phi_{ik}\,Q_{Xi}, \qquad Y_{Rk} = \sum_{i=1}^{N} \Phi_{ik}\,Q_{Yi}, \qquad (k = NB1, NB2)$$

The equations of motion for the auxiliary bearings are derived using the model shown in Fig. 2

$$\begin{aligned} M_{Bk}\ddot{X}_{Bk} + C_{Bk}\dot{X}_{Bk} + K_{Bk}X_{Bk} \\ = F_{nk}\cos\alpha_k - F_{tk}\sin\alpha_k + M_{Bk}\,g, \end{aligned} \qquad (2.a)$$

$$\begin{aligned} M_{Bk}\ddot{Y}_{Bk} + C_{Bk}\dot{Y}_{Bk} + K_{Bk}Y_{Bk} \\ = F_{nk}\sin\alpha_k + F_{tk}\cos\alpha_k, \end{aligned} \qquad (2.b)$$

$$\begin{aligned} J_{Bk}\ddot{\psi}_{Bk} + C_{B\psi k}\dot{\psi}_{Bk} \\ = F_{tk}R_{Bk} - \mu_\psi F_{nk}R_{mk}, \end{aligned} \qquad (2.c)$$

where

$$\alpha_k = tan^{-1}\frac{Y_{Rk} - Y_{Bk}}{X_{Rk} - X_{Bk}}.$$

$$(k = NB1, NB2)$$

At this point, the rotor and the back-up bearings appear to be uncoupled. However, the force vectors $\mathbf{F}_X$ and $\mathbf{F}_Y$ on the right hand sides of equations (1) are partially due to rotor/auxiliary bearing interaction. In fact, we have

$$\begin{aligned} F_{Xk} &= -\,F_{nk}\cos\alpha_k + F_{tk}\sin\alpha_k \\ &\quad + M_k\,g + M_k\,e\,\Omega^2\cos(\Omega t), \\ F_{Yk} &= -\,F_{nk}\sin\alpha_k - F_{tk}\cos\alpha_k \\ &\quad + M_k\,e\,\Omega^2\sin(\Omega t). \end{aligned}$$

The rotor/bearing interaction is represented with the normal force F_{nk}

$$F_{nk} = \begin{cases} K_C\delta_k, & \Delta_k < 0, \\ 0, & \Delta_k \ge 0, \end{cases} \qquad (3.a)$$

where

$$\Delta_k = (X_{Rk} - X_{Bk})\cos\alpha_k + (Y_{Rk} - Y_{Bk})\sin\alpha_k - \delta_k$$

and the Coulomb friction force F_{tk}. As long as there exists slip at the contact point, the friction force obeys

$$F_{tk} = \mu\,F_{nk}. \qquad (3.b)$$

However, when there is no slip at the contact point, the friction forces are solved from equations (1) and (2) using the kinematic constraint that the circumferential velocities of the rotor and the inner-race of the back-up bearing at the contact point equal to each other. At the same time, if this solved friction force exceeds the maximum static friction force ($= \mu_s F_{nk}$), equation (3.b) applys again.

DISCUSSION OF RESULTS

The rotor is modeled with 34 stations (as shown in Fig. 1) and the first four modes (two rigid body and two flexible modes) are included in the simulation model. The two auxiliary bearings are located at nodes 3 and 33, respectively. This arrangement is taken to represent one of the most technically feasible configurations in that it greatly simplifies bearing maintenance. It is assumed that the two auxiliary bearings are identical in terms of stiffness, damping and friction characteristics. Some nominal system parameters used for the simulation study are K_C=2.855e+6, ξ=0.03, R_{mk}=1.1 R_{Bk}, μ_s=0.5 and μ_ψ=0.002. To avoid excessive cluttering of plots, all the results that are presented in this paper correspond to node 3, the location of bearing #1.

Since the total system which includes two bearings and associated friction forces as well as the inner-race motions is rather complicated and requires considerable amount of computer time for the solutions to converge, the friction effect is examined first to see if the model can be further simplified. It turns out that the steady-state results obtained with and without friction are virtually identical. Even the differences in transient responses are quite small, as can be seen in Fig. 3(a) and 3(b). The only remarkable effect is on the transient responses of the inner-race as shown in Fig. 3(c). This observation is confirmed by numerous runs using different system parameters and rotor speeds. The lack of significance of friction may be attributed to several factors. First, the inertia of the inner-race is quite small in comparison to the rotor mass, so vibration of the bearing has little influence on the rotor vibration. Second, ball bearings exhibit quite negligible torsional resistance under normal conditions. As a result, the terms that are related to the friction forces and the rotational motion of the inner race are not included in the simulations that are discussed in the following paragraphs.

The steady-state response characteristics of the system are obtained through numerical integration of the simplified version of governing equations (1) and (2). Near-zero initial conditions are used, simulating situations where the AMBs are functioning properly prior to a system failure. Multiple solutions with other initial conditions are not sought at present.

It is well known from linear analyses that imbalance greatly affects the steady state vibration amplitudes of a rotor system. However, it is observed from the current work that imbalance may also influence frequency content of the rotor responses quite dramatically at certain operating speeds. A typical case with such an imbalance effect is shown in Figs. 4 and 5, where orbits and corresponding frequency spectra of the rotor for different values of imbalance at the speed of $\Omega = 1000$ are plotted. For this particular case, there exist eight ranges of imbalance values that result in eight different types of rotor responses.

For $e \leq 0.0009$, the rotor rotates near the bottom of auxiliary bearings and the responses are predominantly synchronous (Figs. 4(a)-4(b) and 5(a)-5(b)). As imbalance increases, the 2Ω superharmonic component approaches the magnitude order of the synchronous component (Figs. 4(b) and 5(b)). However, the responses are of small amplitude. For $0.0010 \leq e \leq 0.0013$, the responses are dominated by $\Omega/2$ subharmonic components (Figs. 4(c) and 5(c)). In other words, the amplitude of $\Omega/2$ component is greater than that of the synchronous. For $0.0014 \leq e \leq 0.0016$, the $\Omega/2$ subharmonics disappear and the $\Omega/3$ subharmonics become dominant (Figs. 4(d) and 5(d)). So far, the overall amplitude of the responses are not large, the rotor just bounces near the bottom of the auxiliary bearings. For $0.0017 \leq e \leq 0.0027$, the orbits become chaotic-looking (Fig. 4(e)) and the spectrum contains a lot of noise (Fig. 5(e)). In this range of imbalance, the rotor changes from bouncing near the bottom to bouncing around the full clearance of the bearing as imbalance increases. In the middle of this transition range, true chaos is observed. The Poincare map shown in Fig. 6(a) and the frequency spectrum shown in Fig. 6(b) demonstrate that the response has all the characteristics of a chaotic phenomenon. It should be noted that even though the orbits are chaotic looking, the amplitudes are not the largest among all the cases for this particular parametric configuration. For $0.0028 \leq e \leq 0.0034$, the orbits orbits are no longer chaotic-looking (Fig. 4(f)). The spectrum shows they are $\Omega/5$ subharmonic responses (Fig. 5(f)). Notice the amplitudes are the largest for this parametric configuration. For $e = 0.0035$, the amplitude suddenly becomes smaller even though the imbalance has become larger (Fig. 4(g)). And the rotor bounces near the bottom of the auxiliary bearings again. The frequency spectrum shows it is $\Omega/8$ subharmonic response (Fig. 5(g)). For $0.0036 \leq e \leq 0.0042$, the orbits become chaotic-looking again (Fig. 4(h)). But the frequency spectra are very similar to the subharmonic cases (Fig. 5(h)), only with some discrete noise. Finally, for $e \geq 0.0043$, the responses become predominantly synchronous again (Figs. 4(i)-4(j) and 5(i)-5(j)). But this time as imbalance increases, the 2Ω superharmonic component become smaller and smaller (Figs. 4(j) and 5(j)).

Examining all the orbits in terms of amplitudes as imbalance increases, we can see the characteristics of a jump-type phenomenon (Cunningham, 1958). The jump-down takes place around $0.0034 < e < 0035$ where the rotor jumps from full-clearance bouncing to near–bottom bouncing. Further investigation is needed to better understand this type of change.

Imbalance responses at some other operating speeds and for other parametric configurations exhibit similar changes as imbalance varies, though the imbalance ranges and corresponding response types may not be as well defined as in the above cases. In fact, subharmonic responses from $\Omega/2$ through $\Omega/10$ are all observed except $\Omega/9$ as shown in Figs. 7. Surprisingly, those subharmonics are not directly related to the system's natural frequencies as were the cases with other researchers' findings (such as Ehrich, 1988). Moreover, several types of subharmonic responses may occur at a single operating speed. It should be noted that Chen et al. (1993) also reported occurrence of three stable subharmonic responses at a single rotor speed in a SFD supported rotor system but did not provide any explanation for their findings. In their case, even the imbalance did not vary. Apparently, further research is needed to find a mechanism to explain this multi–subharmonic vibration phenomenon. On the other hand, it should be pointed out that these subharmonic responses are not typical cases. While some of them are observed to exist within a certain range of parameters, the majority of them occur only for some specific parametric configurations.

Due to space limitations, results for other parametric configurations are not systematically plotted. A general summation of the observations is presented instead. A common feature among all the responses is that for very small imbalance, the responses are always synchronous. The imbalance range that result in synchronous dominated responses depend on several system parameters. For small back-up bearing stiffness (such as K_B = 0.213e+6) and normal damping (C_B = 157.0), the responses are almost always synchronous. Only $\Omega/2$ subharmonic are observed at a few operating speeds with a very narrow range of imbalance. It should be noted that even though a lower K_B may leads to a better system response, it may also fail to protect the magnetic bearings due to the fact that it could result in a larger rotor orbit-center offset. However, the dramatic response changes discussed above may occur again if the damping becomes small (such as C_B = 57.0) even though the stiffness still remains small. On the other hand, increasing the damping C_B alone may not be able to eliminate those dramatic changes. It is observed that those changes can still occur for C_B being as large as 700.0. Reducing the size of clearance δ may not eliminate the response changes at certain speeds. But it can narrow the operating speed range where those changes occur. For example, response changes are eliminated for $\Omega \geq 1500$ when δ is reduced from 0.002 to 0.001 with all other parameters remaining the same, but response changes still occur for $\Omega \leq 1400$.

It is obvious that rotor responses involving nonsymmetric bearing clearance effect are very complex problems and numerical integration alone is not a sufficient tool to obtain a global picture of the system responses. The harmonic balance method is then used for the investigation of global system behavior. However, it is only attempted for situations with very small imbalance values. In addition, only the 1Ω harmonic is considered. The complex frequency contents associated with medium and large imbalance values makes it a formidable task to apply the harmonic balance method for other cases. Nevertheless, some useful information can be drawn from these results. After all, an adequately balanced rotor system should have very small imbalance under normal conditions.

Fig. 8(a) shows that nonsymmetric clearance effect is equivalent to asymmetric stiffness effect with regards to critical speeds. The clearance actually splits the first critical speed into two pseudo–critical speeds. In the X direction, the gravity force tends to keep the rotor in contact with the bearing at low operating speed. Thus, the apparent stiffness is almost the same as K_B and the pseudo-critical speed is nearly the same as the critical speed for the linear case ($\delta = 0$). But in the Y direction, the clearance results in a lower apparent stiffness and, consequently, an additional lower-value pseudo-critical speed. It is seen that several higher order additional pseudo-critical speeds are created in the operating speed range in addition to the 1st additional pseudo-critical speed. It is noted that the response in the X direction also departs from the linear case at high operating speed. This is because the imbalance force becomes dominant at high rotor speed which in turn makes the gravity force less significant and the clearance effect more important. Fig. 8(b) shows that changing the auxiliary bearing stiffness has little effect on the pseudo–critical speeds of the system. However, for a larger value of imbalance, a higher K_B does leads to a greater tendency of double–valued responses. In each direction, for either a stiffness increase or an imbalance increase, the 1st pseudo–critical peak tend to become a hard–spring type jump and the 2nd one tend to develop into a soft-spring type jump, with the tendency decreasing as the pseudo–critical's order increases.

Fig. 9(a) shows double–valued responses in the Y direction for four different values of clearance. It is seen that a larger clearance results in wider rotor speed range of double–valued responses. It is also observed that as clearance increases, the apparent stiffness decreases and the first pseudo–critical speed shifts to a lower value. Fig. 9(b) shows the double-valued responses in the X direction. Even though the jumps themselves are smaller in magnitude, they are more obvious in trend. Notice how little the change is for the first pseudo-critical speed in the X direction.

Fig. 10(a) shows the influence of auxiliary bearing damping on the double-valued responses in the Y direction. It is observed that the damping has to be quite large to eliminate the double-valued responses associated with the first pseudo-critical speed. Fig. 10(b) shows the influence of C_B on the double-valued responses in the X direction. In both figures, it should be noted that as C_B decreases, the second pseudo-critical speed peak will develop into a soft-spring type jump and the third pseudo-critical speed peak will evolve into a hard-spring type jump.

The system behaviors for higher operating speed range are not shown in Figs. (9) and (10) so that the jump phenomena can be more clearly illustrated. It is also because that the system's responses at high operating speed range with the same parameters are more or less regular, in other words, mainly amplitude changes.

CONCLUSIONS

As a summary of the results discussed above, the following conclusions can be drawn:

1. Imbalance may change the rotor responses dramatically in terms of frequency contents at certain operating speeds, especially under conditions of large clearance, high bearing stiffness and low bearing damping. With imbalance changing, as many as eight different types of responses may occur for a particular parametric configuration at a single operating speed.
2. Subharmonic responses of second order through tenth order are all observed except for the ninth order case. However, the majority of them are not typical cases, and were observed only for quite particular parametric configurations.
3. Chaotic phenomenon is observed to occur occasionally. However, the amplitudes associated with such motion are not among the largest.
4. Nonsymmetric clearance effects influence the critical speeds in a manner similar to asymmetric stiffness effects.
5. Double-valued responses in the form of both hard-spring type jump and soft-spring type jump are observed to be possible at low operating speeds with low auxiliary bearing damping or high imbalance. With large clearances or high bearing stiffness, the jump phenomenon may occur for even relatively small imbalances.
6. The effect of friction between the shaft and the inner race of a rolling element auxiliary bearing on the dynamics of the rotor is quite small and can reasonably be neglected for steady-state analyses.

ACKNOWLEDGEMENT

The authors would like to express their gratitude to S. Klusman of Allison Gas Turbines, Inc. for many helpful discussions and practical advice.

This work was supported by NASA under Grant No. NAG3-1507. The Government has certain rights in this material.

REFERENCES

Bently, D. E., 1974, "Forced Subrotative Speed Dynamic Action of Rotating Machinery," ASME Paper No. 74-PET-16.

Black, H. F., 1968, "Interaction of a Whirling Rotor With a Vibrating Stator Across a Clearance Annulus," *Journal of Engineering Sci ence*, Vol. 10, No. 1, pp. 1-12.

Chen, P. Y. P, Hahn, E. J., and Wang, G. Y., 1993, "Subharmonic Oscillations in Squeeze Film Damped Rotor Bearing Systems Without Centralizing Springs," ASME Paper 93-GT-428.

Childs, D. W., 1979, "Rub-Induced Parametric Excitation in Rotors," ASME *Journal of Mechanical Design*, Vol. 101, pp. 640-644.

Childs, D. W., 1982, "Fractional-Frequency Rotor Motion Due to Nonsymmetric Clearance Effects," ASME *Journal of Engineering for Power*, Vol. 104, pp. 533-541.

Cunningham, W. J., 1958, *Introduction to Nonlinear Analysis*, McGraw-Hill Book Co., New York, NY.

Ehrich, F. F., 1966, "Subharmonic Vibration of Rotors in Bearing Clearance," ASME Paper 66-MD-1.

Ehrich, F. F., 1988, "High Order Subharmonic Response of High Speed Rotors in Bearing Clearance," ASME *Journal of Vibration, Acoustics, Stress, and Reliability in Design*, Vol. 110, pp. 9-16.

Ehrich, F. F., 1991, "Some Observations of Chaotic Vibration Phenomena in High-Speed Rotordynamics," ASME *Journal of Vibration, Acoustics, Stress, and Reliability in Design*, Vol. 113, pp. 50-57.

Gelin, A., Pugnet, J. M., and Hagopian, J. D., 1990, "Dynamic Behavior of Flexible Rotors with Active Magnetic Bearings on Safety Auxiliary Bearings," *Proceedings of 3rd International Conference on Rotordynamics*, Lyon, France, pp. 503-508.

Ishii, T., and Kirk, R. G., 1991, "Transient Response Technique Applied to Active Magnetic Bearing Machinery During Rotor Drop," *DE- Vol. 35, Rotating Machinery and Vehicle Dynamics, ASME*, pp.191-199.

Muszynska, A., 1984, "Partial Lateral Rotor to Stator Rubs, " IMechE Paper No. C281/84.

Yamamoto, T. T., 1954, "On Critical Speeds of a Shaft," *Memoirs of the Faculty of Engineering*, Nagoya University (Japan), Vol. 6, No. 2.

TABLE 1. FEM MODEL DATA

Station (in.)	O.D. (in.)	I.D. (in.)	WT. (lb)	Polar Mom. (lb.in.s^2)
5.400	2.800	2.000	0.000	0.000
5.450	2.800	2.000	5.000	5.000
6.500	2.800	2.000	0.000	0.000
6.505	7.300	6.950	0.100	0.100
7.100	7.300	6.950	0.000	0.000
8.670	7.300	7.120	30.400	425.000
10.900	8.400	8.220	0.000	0.000
13.120	9.300	9.120	0.000	0.000
15.310	10.100	9.920	20.300	538.000
17.280	10.700	10.550	9.150	302.000
18.580	11.200	11.050	0.000	0.000
19.880	11.550	11.400	0.000	0.000
21.120	11.950	11.800	0.000	0.000
22.380	12.150	12.000	41.900	1645.000
23.670	12.400	12.250	0.000	0.000
24.900	12.500	12.350	0.000	0.000
26.120	12.500	12.350	0.000	0.000
27.400	12.500	12.350	22.550	539.000
27.750	12.500	2.500	1.027	0.000
27.800	4.500	2.500	7.733	0.000
32.000	4.500	2.500	25.022	49.761
37.000	4.500	2.500	17.961	0.000
43.000	4.500	2.500	17.961	0.000
48.000	4.500	2.500	16.328	0.000
53.000	4.500	2.500	16.328	0.000
58.000	4.500	2.500	14.614	0.000
61.950	4.500	2.500	6.531	0.000
62.000	6.000	2.500	0.954	0.000
62.405	6.000	5.670	34.935	1216.500
64.600	6.000	5.670	0.000	0.000
67.000	6.000	5.670	117.000	3750.500
69.500	6.000	5.670	0.000	0.000
69.505	2.850	1.250	0.000	0.000
72.500	2.850	1.250	10.197	12.000
73.600	2.850	1.250	0.000	0.000

Modulus of elasticity: E=2.80e+7 psi
Shear Modulus of elasticity: G=1.08e+7 psi

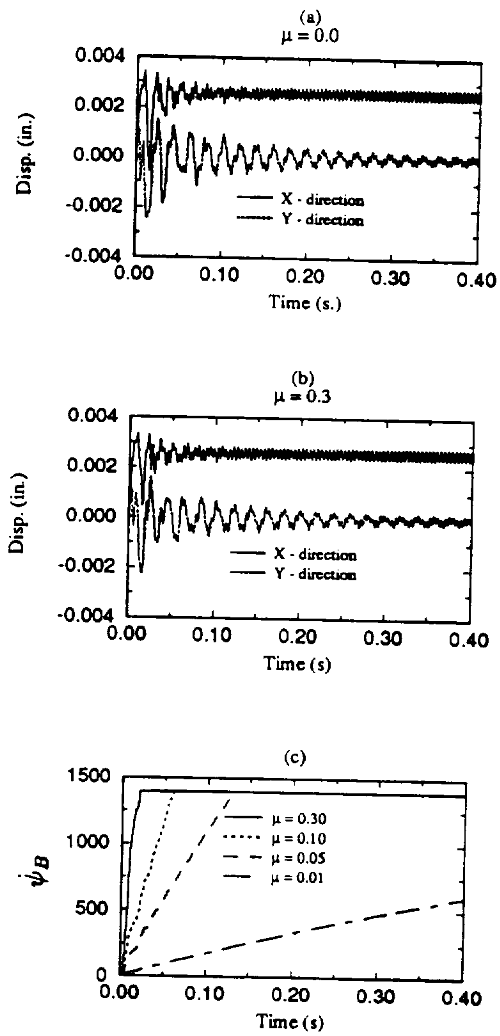

FIG. 3 EFFECTS OF BEARING FRICTION (C_B=157.0, K_B=0.313e+6, Ω=1400, δ=0.002, e=0.0002)

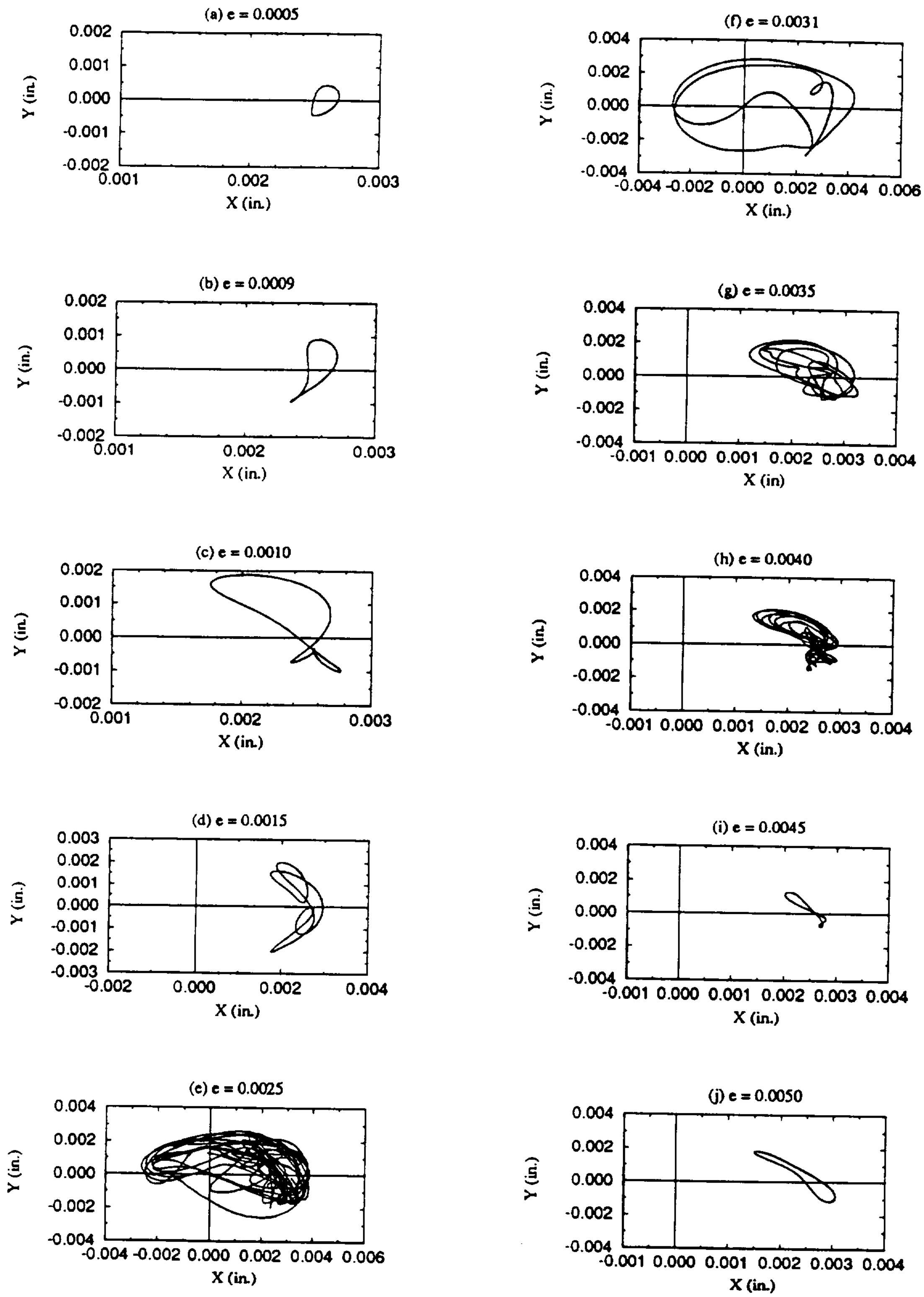

FIG. 4 IMBALANCE RESPONSES - ORBITS
(δ=0.002, K_B=0.313e+6, C_B=157.0)

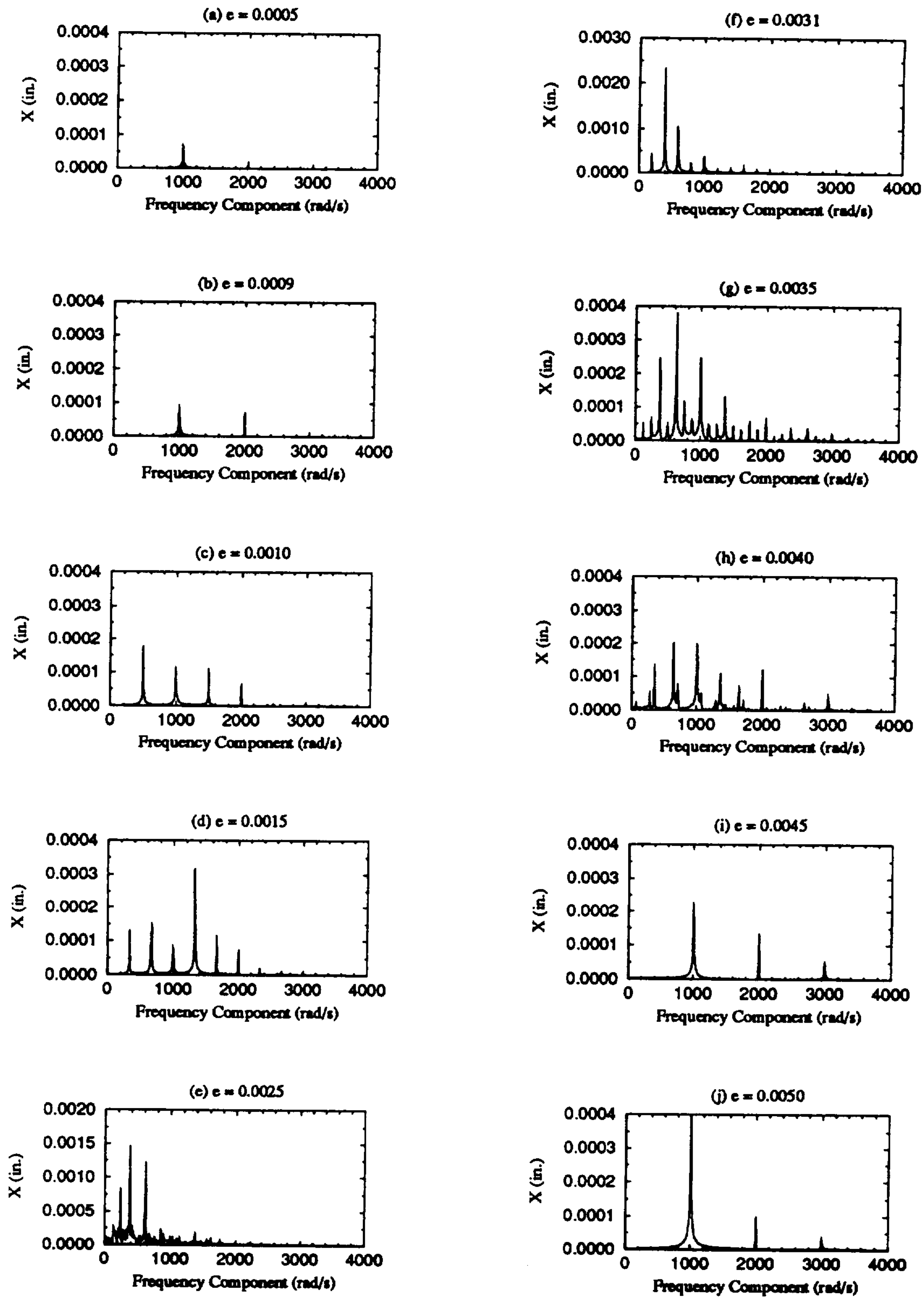

FIG. 5 IMBALANCE RESPONSES - SPECTRA
(δ=0.002, K_B=0.313e+6, C_B=157.0)

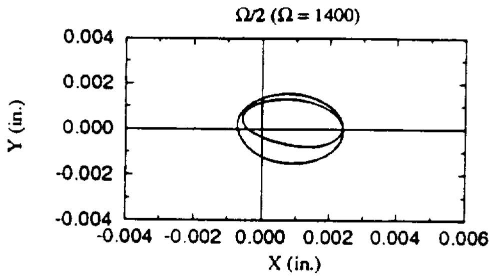

(a) δ=0.001, e=0.0007, C_B=157.0,

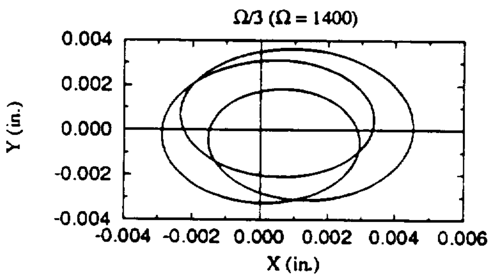

(b) δ=0.001, e=0.0029, C_B=157.0,

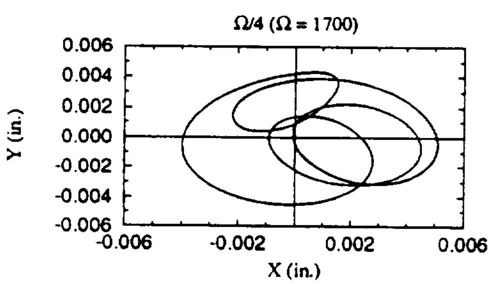

(c) δ=0.002, e=0.00105, C_B=145.0,

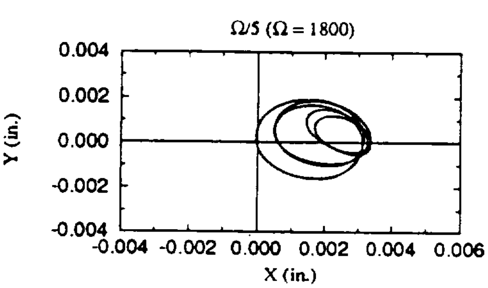

(d) δ=0.002, e=0.00067, C_B=157.0,

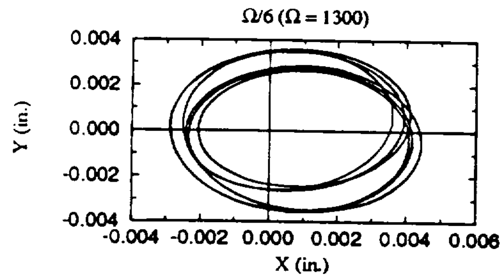

(e) δ=0.002, e=0.0025, C_B=157.0,

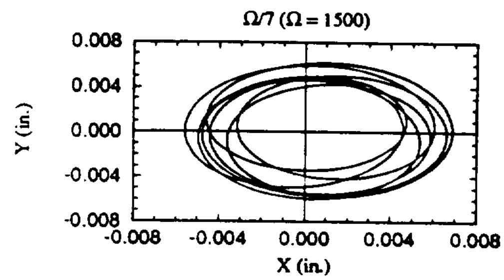

(f) δ=0.002, e=0.0032, C_B=157.0,

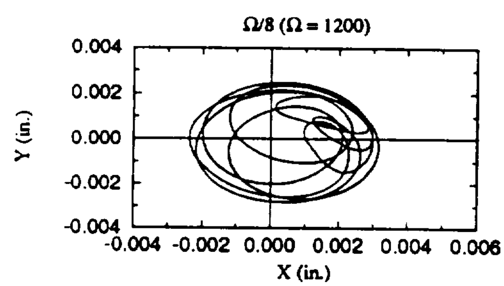

(g) δ=0.001, e=0.0030, C_B=157.0,

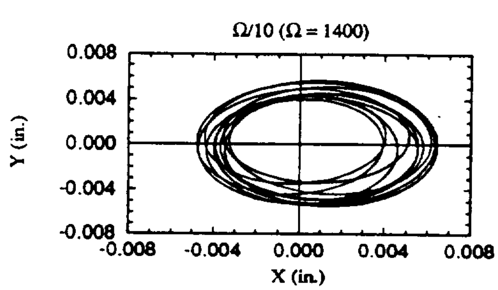

(h) δ=0.002, e=0.00395, C_B=157.0,

FIG. 7 SUBHARMONIC RESPONSES (ORBITS)
(K_B=0.313e+6)

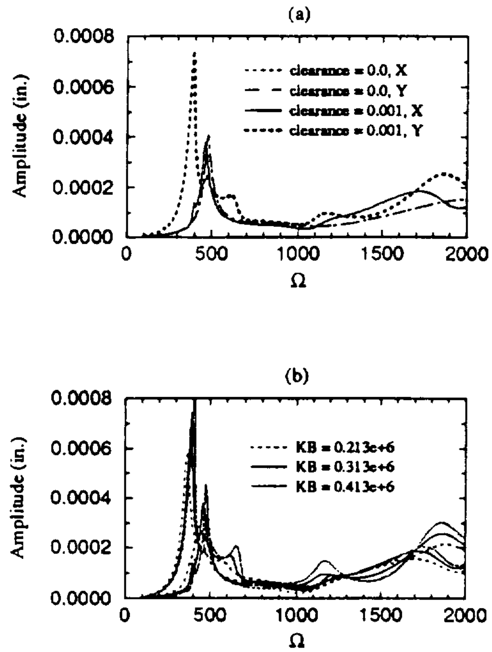

FIG. 8 INFLUENCE ON CRITICAL SPEEDS
(a) e=0.0001, C_B=157.0, K_B=0.313e+6
(b) e=0.0001, C_B=157.0, δ=0.001

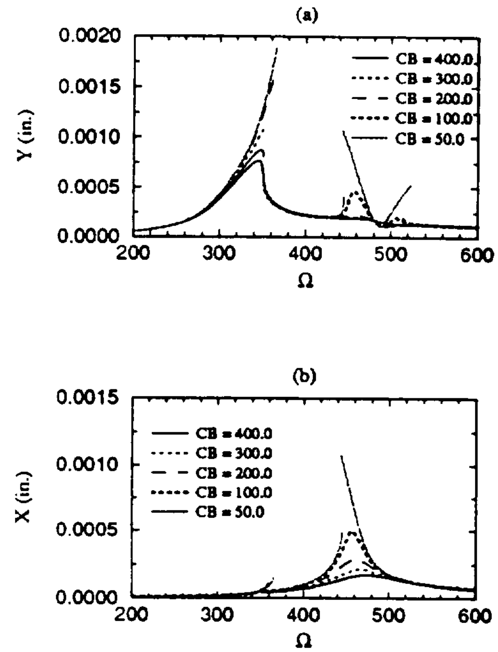

FIG. 10 EFFECTS OF BACK-UP BEARING DAMPING
(δ=0.002, e=0.0001, K_B=0.313e+6)

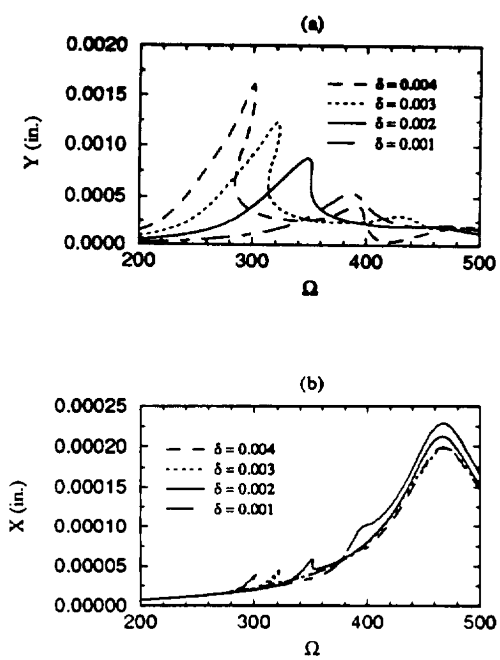

FIG. 9 CLEARANCE EFFECT ON JUMP PHENOMENA
(e=0.0001, K_B=0.313e+6, C_B=300.0)

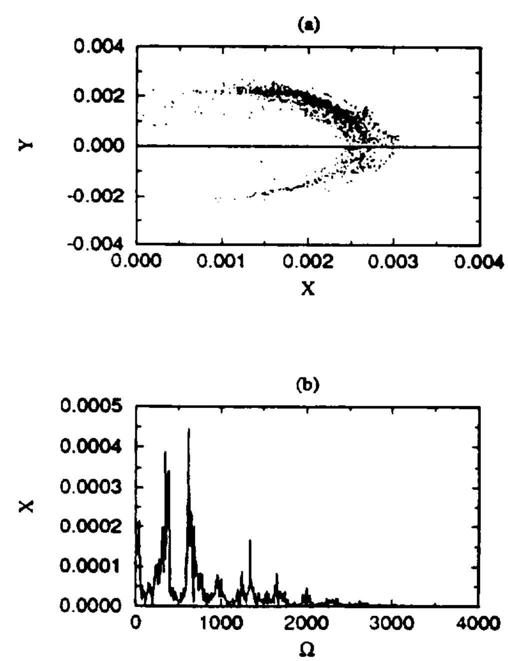

FIG. 6 CHAOTIC RESPONSES (e = 0.0023, δ=0.002, K_B=0.313e+6, C_B=157.0)